Structure and Electrocatalysis of Sputtered RuPt Thin-Film Electrodes

Tae-Wook Kim and Seong-Ju Park*

Department of Materials Science & Engineering, Gwangju Institute of Science & Technology, Gwangju 500-712, South Korea

Lindsay E. Jones† and Michael F. Toney*

Stanford Synchrotron Radiation Laboratory, Stanford Linear Accelerator Center, Menlo Park, California 94025

Kyung-Won Park and Yung-Eun Sung

School of Chemical Engineering & Research Center for Energy Conversion and Storage, Seoul National University, Seoul 151-744, Korea

Received: February 3, 2005; In Final Form: May 3, 2005

The structural and electrochemical properties of RuPt thin-film electrodes fabricated by radio frequency (rf) magnetron sputtering have been investigated. Grazing incidence X-ray diffraction data show a transition from a face-centered cubic (fcc) to hexagonal cubic-packed (hcp) structure as the Ru percentage increases. The transition occurs gradually between 32 and 58% Ru, which is significantly different from the bulk RuPt phase diagram. The catalytic activity of the thin-film electrodes for methanol oxidation shows a broad peak near 40−60% Ru, consistent with previous reports. The relationship between catalytic activity and film structure is discussed and contrasted with previous investigations.

Introduction

Due to various merits such as high energy density, low operating temperature, easy handling, simple processing, and the possibility of applications to micro-fuel cells, direct methanol fuel cells (DMFCs) are currently undergoing rapid development.[1−9] The excellent catalytic activity of platinum-based alloy nanoparticles for methanol oxidation makes this metal electrocatalyst ideal for use as an anode in DMFCs. However, it is well-known that CO, a byproduct in methanol electrooxidation, readily poisons pure platinum at low temperatures. Accordingly, much effort has been reported to design and synthesize Pt-based alloy catalysts by alloying platinum with a second element to enhance its catalytic activity for methanol electrooxidation by eliminating the CO poisoning effect.[10−15] Watanabe et al. have extensively studied Pt-based alloy catalysts designed according to the bifunctional mechanism in DMFCs.[16] Here, oxygen species adsorbed on the alloying element, such as ruthenium, regenerate the CO-poisoned platinum by oxidizing the CO to CO_2.[16,17]

The catalytic activity of RuPt nanoparticles and RuPt alloys is sensitive to catalyst composition and structure. With increasing Ru, the structure of PtRu changes from face-centered cubic (fcc) to hexagonal close-packed (hcp).[18−20] Other research has reported that the composition and structure of supported PtRu nanoparticles affect the catalytic activity.[18,19,21−26] Park et al. observed that 40−60 atom % Ru in RuPt alloy catalysts is optimum for achieving excellent catalytic activity in methanol oxidation.[27] However, there has been little systematic work on the relationship between the structural and electrochemical properties of RuPt thin-film electrocatalysts with a range of structures and compositions.

In this paper, PtRu thin-film electrodes with varying composition were prepared for methanol electrooxidation. Characterization of the thin films was carried out using grazing incidence X-ray diffraction (GIXD) and electrochemical measurements. We relate between structural and electrochemical properties in PtRu thin-film electrodes.

Experimental Section

RuPt thin-film electrodes were grown using a radio frequency (rf) magnetron sputtering system with different conditions. p-Type (100) silicon and indium tin oxide (ITO, Samsung Corning Co, Ltd) were used as substrates to characterize structural and electrochemical properties, respectively. Ruthenium and platinum were used as target materials. To fabricate the RuPt thin-film electrodes, cosputtering was used with different rf powers.[27] Cosputtering was performed under the inert Ar gas at a flow rate of 40 sccm at room temperature for 20 min, which produced films about 130 Å thick. To fabricate RuPt thin-film electrodes with varying composition, guns with metal targets in the rf magnetron sputtering system were controlled as a function of rf power. With increasing rf power of the Ru target gun at a fixed rf power of the platinum gun, the Ru concentration was varied from 0 to 85%. A pure Ru film was also produced.

Grazing incidence X-ray diffraction (GIXD) analysis was carried out using beam line 7-2 at the Stanford Synchrotron Radiation Laboratory. The X-ray energy was either 9 or 10 keV (wavelength (λ) of about 1.38 and 1.24 Å, respectively). In the diffraction measurements, the sample was held to a Huber four-circle diffractometer by a vacuum chuck and was surrounded by a helium atmosphere to reduce unnecessary scattering of X-rays from the air near the sample. An ion chamber, placed after the beam defining slits, was used for incident flux

* To whom correspondence should be addressed.
† Present address: Northeastern University, Boston, MA 02115.

10.1021/jp050616g CCC: $30.25
Published on Web 06/10/2005

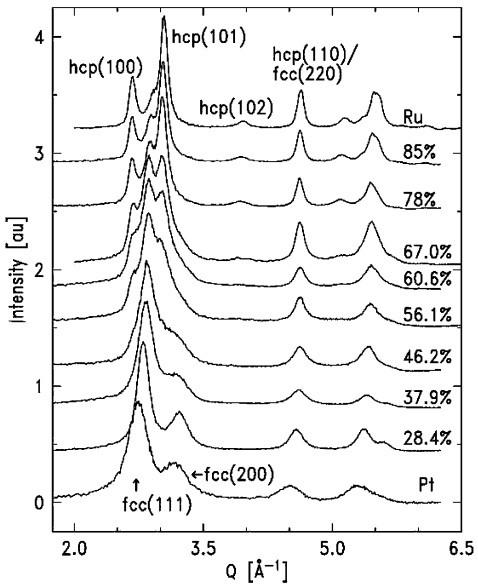

Figure 1. Grazing incidence X-ray diffraction (GIXD) data for RuPt thin-film electrodes. The data are off-set for clarity and are labeled with the Ru percentage.

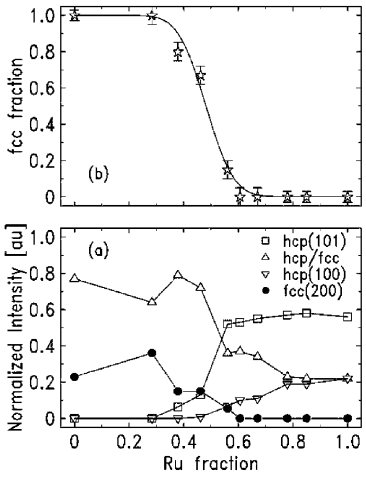

Figure 2. Phase diagram determination for the RuPt thin-film electrodes: (a) normalized integrated intensity versus Ru fraction for several peaks; (b) fcc fraction calculated from normalized intensities.

normalization. The incidence angle was approximately 0.6°, just about the critical angle for total reflection for Pt−Ru alloys. After grazing the sample, the diffracted beams passed through 1 millirad Soller slits, used to define the scattering angle, before reaching the detector.

Electrochemical measurements were made using a three-electrode cell at 25 °C. The deposited RuPt thin-film electrodes, Pt gauze, and an Ag/AgCl electrode (in saturated KCl) were used as the working, counter, and reference electrodes, respectively. All potentials are reported versus the Ag/AgCl (in saturated KCl) reference electrode. All chemicals were of analytical grade. All solutions for electrochemical measurements were stirred constantly and purged with nitrogen gas. Electrochemical experiments were performed with AUTOLAB (Eco Chemie). To identify the electrochemical properties of the RuPt thin-film electrodes, cyclic voltammetry (CV) was performed in the potential range from −0.3 to 0.8 V versus Ag/AgCl in 0.5 M H_2SO_4 solution. The electrocatalytic activity for methanol electrooxidation was measured in 2.0 M CH_3OH in 0.5 M H_2SO_4. The current density was calculated by normalization of the geometric area of the thin-film electrode exposed to the solution.

Results

Structural Properties of RuPt Thin-Film Electrodes by GIXD Analysis. Before describing our data, it is useful to briefly review the bulk phase diagram for Ru−Pt alloys.[20,28,29] For Ru atomic fractions up to 62%, Pt and Ru form a solid solution with a face-centered cubic (fcc) structure, while the lattice parameter decreases from 3.925 (pure Pt) to 3.85 Å at 62% Ru. Above 80% Ru, a solid solution with a hexagonal close-packed (hcp) structure forms. Between these compositions, the alloys form a two-phase region of mixed fcc and hcp.

Figure 1 shows the GIXD data for well-defined RuPt thin-film electrodes as a function of increasing Ru from bottom to top. These data are plotted as a function of the scattering vector $Q = (4\pi/\lambda) \sin \theta$, where θ is half the scattering angle. Some of the diffraction peaks for both fcc and hcp alloys are noted. This figure reveals several important points. First, as the Ru fraction increases, the crystal structure of the film changes from fcc to hcp. Below about 40% Ru, the films are fcc, while, above about 65% Ru, the films adopt a hcp structure. Between these compositions, the films appear to be mixed fcc and hcp. Second, the diffraction peaks shift to higher Q with increasing Ru, which is due to a decrease in the lattice parameters. Last, the peaks are rather broad, which implies a small grain size. We have also measured the crystallographic texture in these films and found that for the fcc and mixed phase films there is a weak fcc(111)/hcp(002) texture, while for the hcp films there is a somewhat stronger hcp(002) texture (which is evident by the weak hcp(002) peaks in Figure 1).

From the data in Figure 1, we can extract the approximate percentage of fcc and hcp alloys present in the thin films. Figure 2a shows the normalized, integrated intensity of the hcp(100), fcc(111)/hcp(002) (which are indistinguishable), hcp (101), and fcc(200) peaks as a function of Ru concentration. The intensities are normalized by dividing the peak intensities by the sum of the intensities of these four peaks; this removes differences in the raw data due to different X-ray energies and slightly different incidence angles. As can be seen, the trends in the intensities of the fcc peaks and the hcp peaks are mutually consistent, which confirms the validity of this approach for estimating the phase fractions. We can quantify this further by taking into account the atomic form factors, multiplicities, and Lorenz polarization factors and calculating the fcc fraction from the hcp(101) and fcc(200) peaks, which are strong and clearly distinct (i.e., do not overlap other peaks). This is shown in Figure 2b. As is apparent the hcp phase begins to form near 40% Ru and is complete just above 60% Ru. This is different from the expectations of the bulk phase diagram, and this is highlighted in Figure 3, which shows both the bulk[20,28,29] and our "thin-film phase diagram". The cosputtering method shifts the phase diagram significantly, and the phase transition boundary changes markedly from 62−80% Ru in the bulk to approximately 32−58% Ru in the films. This will be contrasted with the electrochemical behavior of the alloys below.

Before turning to the electrochemistry, it is interesting to examine the lattice parameters, and these are shown in Figure 4 as a function of Ru fraction. The solid symbols are the lattice parameters calculated from the GIXD data (Figure 1), while the open symbols are calculated from the specular (usual $\theta/2\theta$ geometry) data (not shown). The solid lines are values for the bulk fcc and hcp phases,[20] while the dashed lines are guides to the data. The error bars are larger in the mixed phase region,

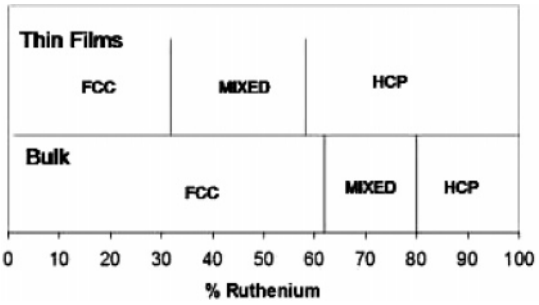

Figure 3. RuPt phase diagram. The data for thin films (under our growth conditions) are constructed from Figure 2, while the bulk data is from Gasteiger.[20] The thin-film phase diagram is shifted to the left and has a wider mixed phase.

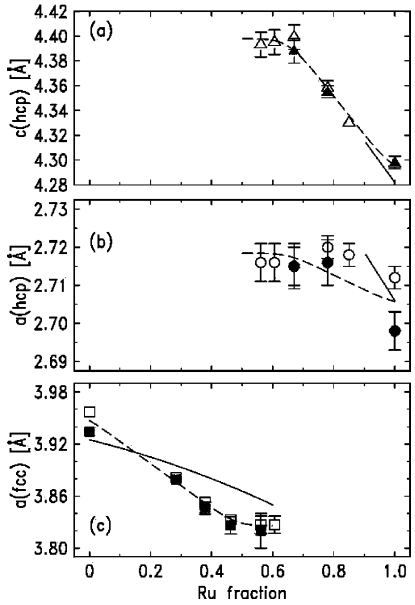

Figure 4. Lattice parameters from diffraction data of RuPt thin-film electrodes. The open symbols are the in-plane data, while the closed symbols are specular data. The solid lines are data for bulk alloys, while the dashed lines are guides.

because many of the fcc and hcp peaks overlap. In both the hcp and fcc phases, the lattice parameters decrease as the percentage of Ru increases, with the smaller Ru atoms substituting for Pt. For the hcp phase (Figure 4a and b), *a* and *c* are not too different from the bulk values. However, for the fcc phase (Figure 4c), the thin-film data show a different trend from the bulk with a more pronounced dependence on Ru fraction. The film two-phase region (32−58%) manifests itself as a plateau in the lattice parameters. Note that since the thin-film and bulk lattice parameters are different, one cannot use empirically determined lattice parameters to infer film composition. This is an important observation, since lattice parameter measurements have routinely been used to deduce film composition[7,27] for nanoparticle catalysts. Our results in Figure 4 show that this approach could result in errors in composition as large as 10%, and hence, this method should be used cautiously.

Electrochemical Properties of RuPt Thin-Film Electrodes. The GIXD data show the dependence of the structural properties on film composition and the difference between bulk RuPt alloy and thin-film phase diagrams. Since RuPt nanoparticles with different compositions have distinct electrochemical properties, especially for methanol electrooxidation, the electrochemical properties of our RuPt thin films will also depend on composition, which, in turn, is dependent on the rf power of Pt and Ru

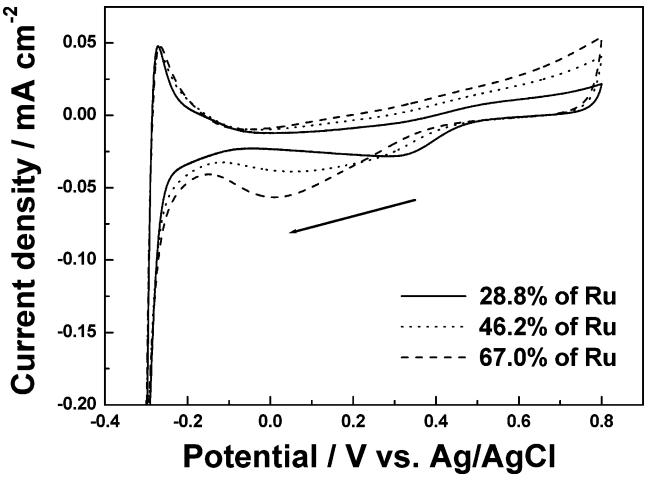

Figure 5. Cyclic voltammograms of RuPt thin-film electrodes in 0.5 M H_2SO_4 solution. The solid, dotted, and dashed lines represent 28.8, 46.2, and 67.0% Ru, respectively. The potential range is from −0.3 to 0.8 V vs the Ag/AgCl reference electrode with a 20 mV/s scan rate.

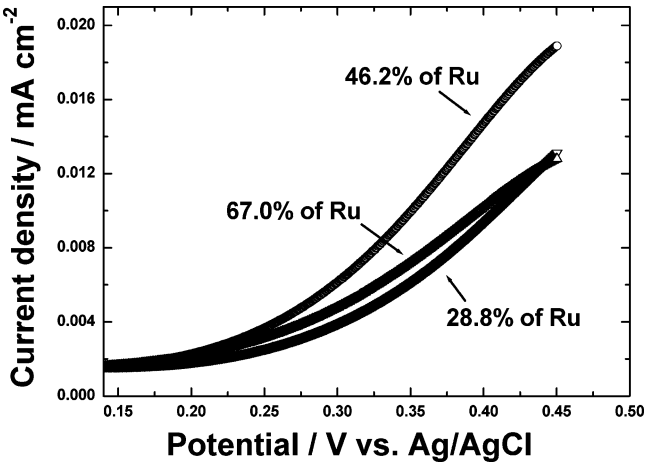

Figure 6. Methanol electrooxidation current density of RuPt thin-film electrodes which contain 28.8, 46.2, and 67.0% Ru in a solution of 2.0 M CH_3OH in 0.5 M H_2SO_4. The potential range is from 0.14 to 0.45 V vs the Ag/AgCl reference electrode with a 20 mV/s scan rate.

sputtering targets. Also, since all of the RuPt thin films with different compositions showed almost the same value of root mean square (rms) roughness, about 3.5 nm, the distinct electrochemical properties are not due to roughness changes.

This is the case as shown in Figure 5, which plots the cyclic voltammetry (CV) for the thin-film electrodes with several compositions. Compared with the solid line (28.8% Ru), the dotted line (46.2% Ru) shows a larger double layer thickness in the potential range 0.0−0.4 V and a lower surface oxide reduction potential (shown by the arrow in Figure 5). For the 67.0% Ru alloy (dashed line in Figure 5), the double layer is significantly thicker and the surface oxide reduction potential is much lower. The thickness of the double layer region increases with increasing Ru composition because of the increased hydrophilicity of Ru. The surface oxide reduction potential decreases due to the slow kinetics of Ru in RuPt thin-film electrodes for surface oxide reduction.

Figure 6 shows a plot of the current density for methanol electrooxidation with respect to applied potential for RuPt thin-film electrodes containing 28.8, 46.2, and 67.0% Ru. As is apparent, the thin film with 46.2% Ru has the highest catalytic activity, consistent with studies on similar systems.[27] Recall that

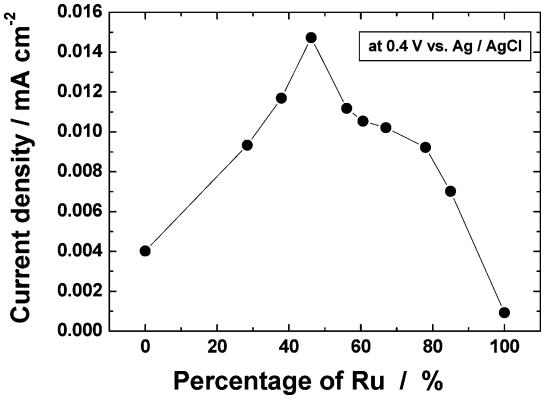

Figure 7. Methanol electrooxidation current density of RuPt thin-film electrodes in a solution of 2.0 M CH_3OH in 0.5 M H_2SO_4 at 0.4 V vs the Ag/AgCl reference electrode. The current is normalized by the geometric area of the film exposed to the solution.

this film has a mixed fcc and hcp structure. Figure 7 shows the Ru dependence of the methanol electrooxidation current density of RuPt thin-film electrodes at 0.4 V. As is apparent, there is a broad maximum in the catalytic activity in the range 40−60 atom % Ru, with the highest catalytic activity in the thin film containing 46.2% Ru.

Discussion

It has been reported that for supported and unsupported nanoparticle RuPt catalysts 40−60% Ru gives the optimum catalytic activity for methanol oxidation.[24−27,30,31] Similarly, in bulk RuPt alloys, the best catalytic activity is found for ≈50% Ru in the bulk alloy.[32,33] In these articles, the RuPt alloy is in the fcc phase. Indeed, it has been reported that the fcc phase is stabilized in RuPt nanoparticles beyond the bulk stability limit (62% Ru). For example, for 2.5 nm RuPt nanoparticles prepared on carbon supports by the reduction of molecular precursors, mostly fcc nanoparticles are obtained for up to 80 atom % Ru.[21] Similarly, for 2.5−4.5 nm nanoparticles prepared by water-in-oil microemulsions, an fcc alloy is found up to at least 65 atom % Ru.[22]

Our sputtered films, however, seem to be different from these nanoparticles in that the fcc phase is less stable than the bulk and the hcp phase is formed at a low Ru concentration (see Figure 3). Despite this structural difference, we also find, consistent with supported and unsupported RuPt catalysts, that the maximum in the catalytic activity for methanol electrooxidation lies in the range 40−60% Ru (see Figure 7). These results suggest that the presence of hcp RuPt does not affect methanol oxidation in contrast to previous assumptions.[23] Our findings are consistent with other work on sputtered WO_x−RuPt nanostructures in that a 40−60% Ru alloy gives the best catalytic activity but is a mixed fcc/hcp phase.[34]

According to the bifunctional mechanism,[16] oxygen containing species adsorbed on Ru surface atoms react with CO-poisoned platinum sites, yielding CO_2 and regenerating an active Pt site. The arrangement of surface atoms is hence important in this process. This arrangement depends on the bulk crystal structure and the exposed crystal face. For example, for fcc-(111) and hcp(002), the faces have the same hexagonal surface, but fcc(100) is square and hcp(100) is rectangular. Thus, the bulk structure will have an influence on the catalytic mechanism. In modeling studies of this process,[35,36] the alloys are assumed to be fcc. Since the arrangement of surface atoms depends on the bulk structure and crystal face exposed, our results show this assumption is necessarily not valid for all electrocatalysts. This result can be important with respect to the mechanism of Ru enhancement.

Summary and Conclusions

To understand the structural and electrochemical properties of PtRu for methanol electrooxidation, we prepared sputtered PtRu thin-film electrodes with different compositions and structures. From the GIXD data, we observed that the RuPt thin-film electrodes evolved from fcc through mixed fcc/hcp to hcp structures as the Ru concentration increased. The phase diagram for sputtered RuPt thin-film electrodes was significantly different from the bulk phase diagram, with the fcc-to-hcp transition in the films occurring at 32−58% Ru, while the bulk transition is at 62−80% Ru. In the electrochemical measurements, the thin-film electrodes showed a broad region of maximum catalytic activity for methanol oxidation at 40−60% Ru. Significantly, the RuPt electrodes with mixed phase showed excellent catalytic activity.

Our results show that the presence of hcp RuPt does not adversely affect the catalytic activity of the alloys for methanol oxidation and that the assumption of an fcc structure for RuPt alloys is not necessarily valid for low Ru concentrations. They further show that the bulk phase diagram is not a good guide to the thin-film structure for these materials. Finally, the existence of strain shows that one cannot use the diffraction peak positions to infer the Ru concentration in the alloys.

Acknowledgment. Portions of this research were carried out at the Stanford Synchrotron Radiation Laboratory, a national user facility operated by Stanford University on behalf of the U.S. Department of Energy (DOE), Office of Basic Energy Sciences. L.E.J. thanks the DOE Office of Science, Science Education and Workforce Development Division for a Science Undergraduate Laboratory Internship.

References and Notes

(1) Harth, M. P.; Hards, G. A. *Platinum Met. Rev.* **1996**, *40*, 150.
(2) Oetjen, H.-F.; Schmidt, V. M.; Stimming, U.; Trila, F. *J. Electrochem. Soc.* **1996**, *143*, 3838.
(3) Hamnett, A. *Catal. Today* **1997**, *38*, 445.
(4) Reddington, E.; Sapienza, A.; Gurau, B.; Viswanathan, R.; Sarangapani, S.; Somtkin, E. S.; Mallouk, T. E. *Science* **1998**, *280*, 1735.
(5) Ross, P. N. In *Electrocatalysis*; Lipkowski, J.; Wiley-VCH: New York, 1998; Chapter 2.
(6) Wieckowski, A., Ed. *Interfacial Electrochemistry*; Marcel-Dekker: New York, 1999; Chapters 44−51.
(7) Park, K.-W.; Choi, J.-H.; Kwon, B.-K.; Lee, S.-A.; Sung, Y.-E.; Ha, H.-Y.; Hong, S.-A.; Kim, H.; Wieckowski, A. *J. Phys. Chem. B* **2002**, *106*, 1869.
(8) Lee, S.-A.; Park, K.-W.; Choi, J.-H.; Kwon, B.-K.; Sung, Y.-E. *J. Electrochem. Soc.* **2002**, *149*, 1299.
(9) Park, K.-W.; Ahn, K.-S.; Choi, J.-H.; Nah, Y.-C.; Kim, Y.-M.; Sung, Y.-E. *Appl. Phys. Lett.* **2002**, *81*, 907.
(10) Radmilovic, V.; Gasteiger, H. A.; Ross, P. N. *J. Catal.* **1995**, *154*, 96.
(11) Hammet, A.; Kennedy, B. J.; Wagner, F. E. *J. Catal.* **1990**, *124*, 30.
(12) Zhang, H.; Wang, Y.; Fachini, E. S.; Cabrera, C. R. *Elecrtochem. Solid-State Lett.* **1999**, *2*, 437.
(13) Ishikawa, Y.; Liao, M. S.; Cabrera, C. R. *Surf. Sci.* **2000**, *66*, 463.
(14) Shen, P. K.; Tseung, A. C. C. *J. Electrochem. Soc.* **1994**, *141*, 382.
(15) Ley, K. L.; Liu, R.; Pu, C.; Fan, Q.; Leyarovska, N.; Segre, C.; Smotkin, E. S. *J. Electrochem.* Soc. **1997**, *144*, 1543.
(16) Watanabe, M.; Motoo, S. *J. Electroanal. Chem.* **1975**, *60*, 276.
(17) Herrero, E.; Franaszczuk, K.; Wiekowski, A. *J. Phys. Chem. B* **1994**, *98*, 5074.
(18) Pan, C.; Dassenoy, F.; Casanove, M. J.; Philippot, K.; Amiens, C.; Lecante, P.; Mosset, A.; Chaudret, B. *J. Phys. Chem. B* **2003**, *103*, 10098.
(19) Antolini, E. *Mate. Chem. Phys.* **2003**, *78*, 563.
(20) Gasteiger, H. A.; Markovic, N.; Ross, P. N.; Cairns, E. J. *J. Phys. Chem.* **1993**, *97*, 12020.
(21) Zhang, X.; Chan, K.-Y. *Chem. Mater.* **2003**, *15*, 451.

(22) Hills, C. W.; Mack, N. H.; Nuzzo, R. G. *J. Phys. Chem. B* **2003**, *107*, 2626.
(23) Gurau, B.; Viswanathan, R.; Liu, R.; Lafrenz, T. J.; Ley, K. L.; Smotkin, E. S.; Reddington, E.; Sapienza, A.; Chan, B. C.; Mallouk, T. E.; Sarangapani, S. *J. Phys. Chem. B* **1998**, *102*, 9997.
(24) Appleby, A. J. In *The Electrocatalysis of Fuel Cell Reactions*; Dudley, R., O'Grady, W., Srinivasan, S., Eds.; The Electrochemical Soceity Softbound Proceedings Series PV 97-2; Princeton, NJ, 1979; p 23.
(25) Goodenough, J. B.; Hamnett, A.; Kennedy, B. J.; Manoharan, R.; Weeks, S. A. *J. Electroanal. Chem.* **1988**, *240*, 133.
(26) Chu, D.; Gilman, S. *J. Electroanal. Chem.* **1996**, *143*, 1685.
(27) Park, K.-W.; Choi, J.-H.; Ahn, K.-S.; Sung, Y.-E. *J. Phys. Chem. B* **2004**, *108*, 5989.
(28) Ageev, N. V.; Kuznetsov, V. G. *Izv. Akad. Nauk., Ser. Khim.* **1937**, *6*, 753.
(29) Hutchinson, J. M. *Platinum Met. Rev.* **1972**, *16*, 88.
(30) Jusys, Z.; Kaiser, J.; Behm, R. J. *Electrochim. Acta* **2002**, *47*, 3693.
(31) Arico, A. S.; Antonucci, P. L.; Modica, E.; Baglio, V.; Kim, H.; Antonucci, V. *Electrochim. Acta* **2002**, *47*, 3723.
(32) Gasteiger, H. A.; Markovic, N.; Ross, P. N.; Cairns, E. J. *J. Electrochem. Soc.* **1994**, *141*, 1795.
(33) Gasteiger, H. A.; Ross, P. N.; Cairns, E. J. *Surf. Sci.* **1993**, *293*, 67.
(34) Park, K. W.; Sung, Y. E.; Toney, M. F. Unpublished results.
(35) Christov, M.; Sundmacher, K. *Surf. Sci.* **2003**, *547*, 1.
(36) Desai, S. K.; Neurock, M. *Phys. Rev. B* **2003**, *68*, 075420.